ACCESS
Arctic Climate Change
Economy and Society

Project no. 265863

ACCESS

Arctic Climate Change, Economy and Society

Instrument: Collaborative Project
Thematic Priority: Ocean.2010-1 "Quantification of climate change impacts on economic sectors in the Arctic"

D1.26 – Report on ridge shapes and distributions for extreme value analyses in WP2, WP4 and under-ice ecosystems in WP3

Due date of deliverable: **31/12/2013**

Actual submission date: 11/2/2014

Used Person/months:12

Authors: Prof P Wadhams, Dr M Doble

Start date of project: **March 1st, 2011** Duration: **48 months**

Organisation name of lead contractor for this deliverable: **UCAM**

Project co-funded by the European Commission within the Seventh Framework Programme (2007-2013)		
Dissemination Level		
PU	Public	X
PP	Restricted to other programme participants (including the Commission Services)	
RE	Restricted to a group specified by the consortium (including the Commission Services)	
CO	Confidential, only for members of the consortium (including the Commission Services)	

Contents

1. Purpose of study

The geometrical characteristics of the underside of Arctic sea ice have always been difficult to determine. The best available data have come from submarine transects under ice and have consisted of single-beam upward looking sonar (ULS) profiles with, at best, additional information on three-dimensional structure from sidescan sonar (Wadhams, 1978, 1988). The very best that could be done to resolve the actual shape of pressure ridges was to use sidescan sonar to estimate the angle at which the ridge axis crosses the track of the submarine, then to use this information to correct the one-dimensional sonar profile of the ridge so as to achieve a single slice of the ridge measured at right angles to the ridge crest axis (Davis and Wadhams, 1995).

The need for better information is apparent. The estimation of the design load for an offshore structure involves finding the geometry of the most formidable multi-year pressure ridge system that is likely to impact the structure in 100 or 1000 years, this geometry involving the depth of the ridge crest, shape of the ridge and length of the ridge as well as the strength properties of the ice comprising it. These parameters can be estimated by extrapolation from the statistical properties of observable ridges and by applying the statistics of extreme values to estimate the most severe ridge occurring in a given time interval or spatial extent (e.g. Wadhams, 1983, for the analogous case of ice scour depth statistics). The difficulty lies in acquiring the necessary data on existing ridges.

A breakthrough in this area occurred in 2004, when the author of this study obtained the first true 3-D data of the ice underside using an inverted multibeam sonar looking upwards from an autonomous underwater vehicle or AUV (Wadhams et al., 2006). Since then the same author has obtained further very extensive data at lower resolution using the same system fitted to a British naval submarine in March 2007 (Wadhams, 2008), and more restricted data at high resolution using a smaller AUV deployed through holes in the ice cover in 2007 and 2008 (Wadhams and Doble, 2008; Doble *et al*., 2009).

For this deliverable we examine statistically the geometrical properties of pressure ridges derived from the 2004 dataset to demonstrate the additional insight now available from 3-D datasets. The 2004 AUV mission offers higher quality imagery than that from the 2007 submarine mission (subject to data drop outs due to cable leakage), so we focus on use of this dataset to develop the analysis technique, with an analysis of the 2007 data to follow later in the project when extensive data reprocessing is complete.

2. Location of study

The vehicle which generated the data was the UK Autosub-II AUV of Southampton Oceanography Centre, which the authors took to Fram Strait and NE Greenland aboard RRS *James Clark Ross* in August 2004, undertaking a program of under-ice exploration on the Greenland continental shelf from 79°N northwards. This shelf is the widest in Greenland, and contains the shallow Belgica and Ob' Banks (Figure 1, overleaf). To the east lies Fram Strait, where the southward-flowing East Greenland Current (EGC) carries polar ice from the Arctic Basin. To the west the

Belgica Bank is separated from the Greenland coast by a system of connected troughs (Belgica, Norske, and Westwind) with outlets to south and north.

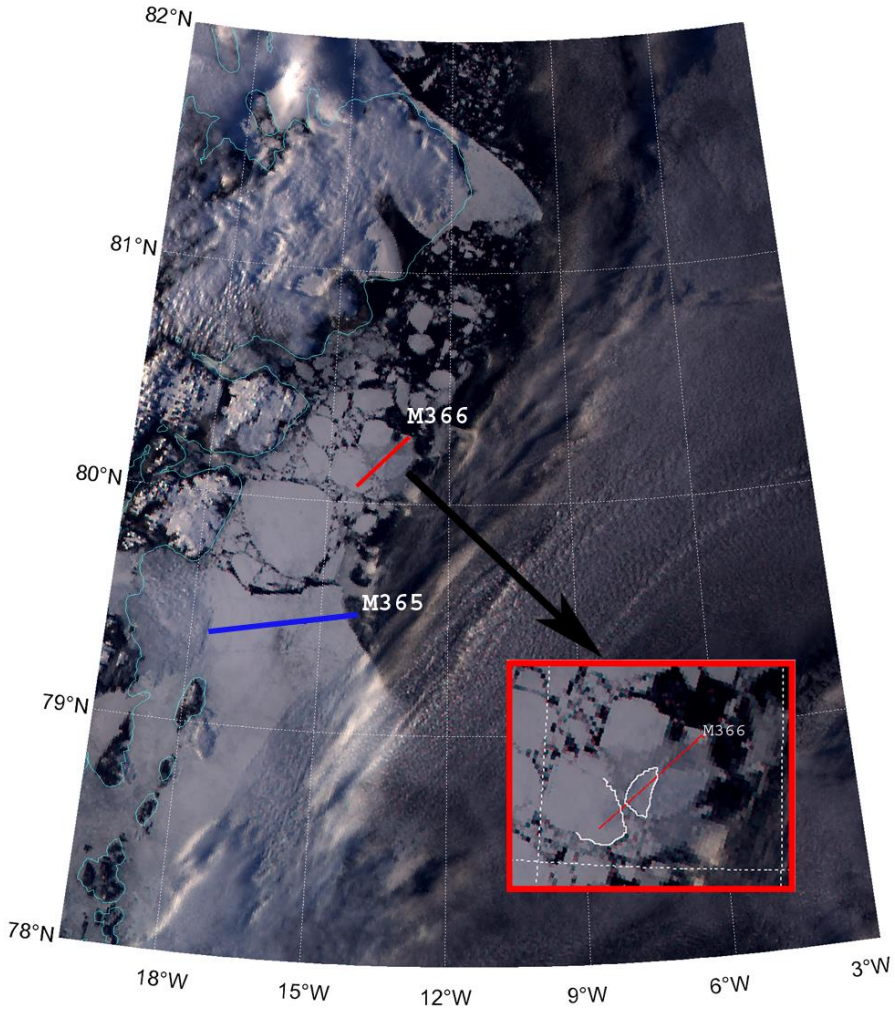

Figure 1: MODIS visual image of ice extent on NE Greenland shelf, 12 August 2004, showing extent of fast ice cover and the locations of Autosub missions used in this study.

The Belgica Bank is very shallow in places and was recently found to contain small low-lying islands (Mohr and Forsberg, 2001) such as Tobias Island, an ice-push feature resembling Alaskan barrier islands. Ice conditions over the bank-trough system are very heavy. Ridged polar ice from the EGC grounds on Belgica Bank together with broken-out thin tabular icebergs from nearby Greenland glaciers such as the 79 Glacier and the Zachariae Isstrøm, where a major iceberg breakout was observed in 2003. These grounded masses form pinning points for a locally-grown fast ice sheet which extends across the Norske Trough to the Greenland coast, known as the Norske Øer Ice Barrier (NØIB) (Reeh et al., 2001). Complete breakup of NØIB was once rare,

occurring about every 50 years (Higgins, 1991), but recently the NØIB disintegrated in the summers of 1997, 2002, 2003 and 2004. North of the ice barrier is a polynya near Ob' Bank known as the Northeast Water (NEW), lasting from May/June until September (Böhm et al., 1997).

A series of Autosub missions was despatched westwards from Belgica Bank fast ice edge towards the Greenland coast, passing first through the shallow water zone north of the Northwind Shoal, then to the deeper Norske Trough, and close to the Greenland coast. The missions were up to 25 hours in duration, i.e. 150 km of track. While Autosub was under the ice the shipboard team ran lines of drilled holes at 5 m intervals along the axis of the vehicle's track near the ice edge and took ice cores. Of these, data from mission 365 are used in this study. The ship then moved northward to 80° 17'N 13° 01'W, to Westwind Trough and the area of the NEW Polynya. Mission 366 (also used in this study) was then carried out from the fast ice edge. Figure 2 shows oceanographic data obtained by the AUV from the 68 km outward track of M365 (see fig. 1 for track), run at 40 m depth. A similar record from mission 366 is shown in Figure 3.

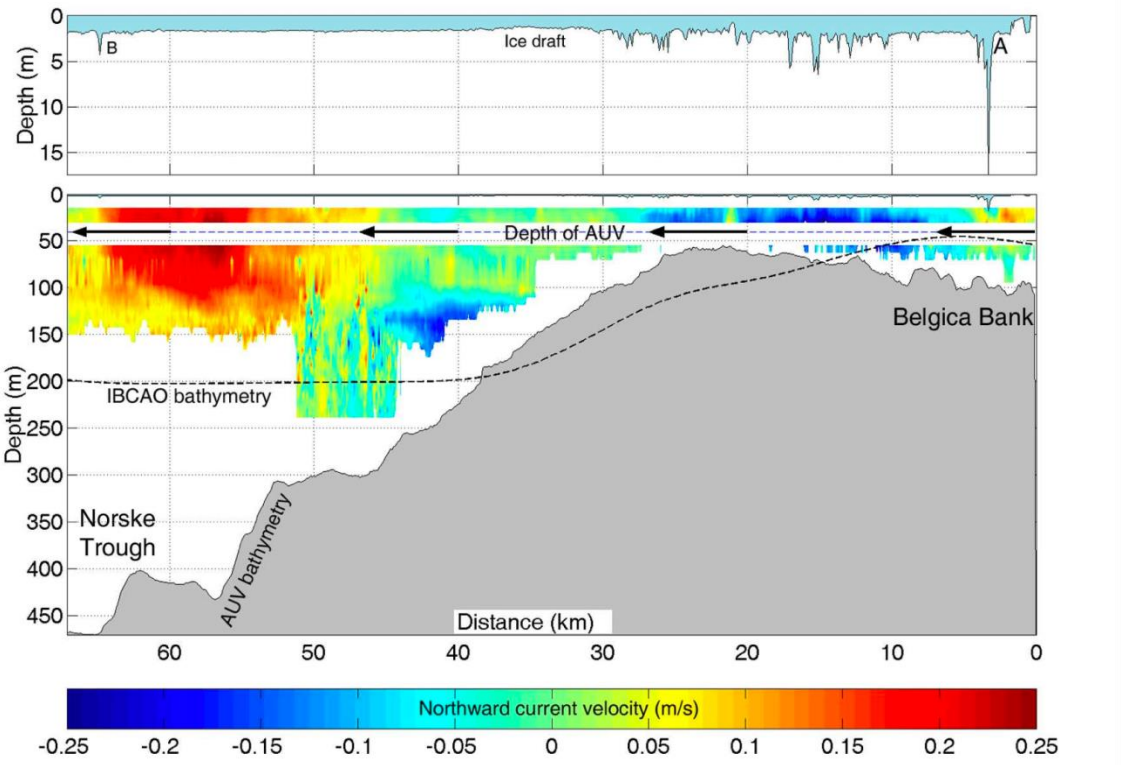

Figure 2: The outward track of mission 365, 21-22 August 2004, run at 40 m depth. The top profile is ice draft measured at crude resolution by upward-looking ADCP; A and B are ridges 1 and 6 in the present study, whose depths are underestimated by the ADCP. Note smooth undeformed ice over Norske Trough. The bottom profile is the seabed topography measured by Autosub compared with the IBCAO bathymetry (dashed line). The coloured masses are N-S velocity components measured by the downward looking ADCP aboard Autosub. The red area is a strong northward current in the Trough, the Northeast Greenland Coastal Current (NGCC); the blue area is a hitherto unrecognised southward current on the western flank of Belgica Bank.

Firstly, we see that the bathymetry available from IBCAO (International Bathymetric Chart of the Arctic Ocean), itself updated in 2001 (Jakobsson et al, 2000), is deficient, showing deeper water over Belgica Bank and shallower water over Norske Trough than found by Autosub, and also much less detailed topography. The undulations in bottom topography near the beginning of Autosub's track (0-15 km) are probably iceberg scours, similar to others seen in nearby surveys by *James Clark Ross's* shipborne multibeam system. Autosub shows the Norske Trough to be at least 460 m deep near its western end, while the IBCAO bathymetry shows 200 m.

The vehicle was equipped with upward- and downward-looking ADCPs which show the northward velocity component of the water, normally detectable down to depths of 100-150 m (dependent on the concentration of scatterers in the water column). The red zone on the left of the figure shows that at 50-60 km penetration, and at water depths from the surface to 100 m, there is a strong northward current component of 0.2–0.25 m s^{-1}, while at 35-45 km penetration, and at water depths of 100-120 m, there is a strong southward component of 0.15–0.25 m s^{-1}. The shelf circulation in this area was first described by Bourke et al. (1987) and refined by the International Arctic Polynya Programme (Hirche and Deming, 1997). They defined a northward-flowing Northeast Greenland Coastal Current (NGCC) within the trough system. We can identify the northward current seen by Autosub with the NGCC but the southward current is a hitherto unrecognized counter-current.

The ice draft record in Figure 2 is a low-resolution profile obtained by upward ADCP. In general the coarse resolution is due to the wide beam-width of the ADCP's sonar. It only becomes an issue if the insonified area falls partly under level and deformed ice. Then the ice draft obtained will be smeared towards a thinner measurement. For instance, the 33 m ridge was shown on the ADCP as only 15 m deep. It shows that the Belgica Bank shallows were covered with ridged ice, while the Norske Trough was covered by an undeformed, locally-grown fast ice sheet less than 2 m thick, with a second small area of ridging near Greenland.

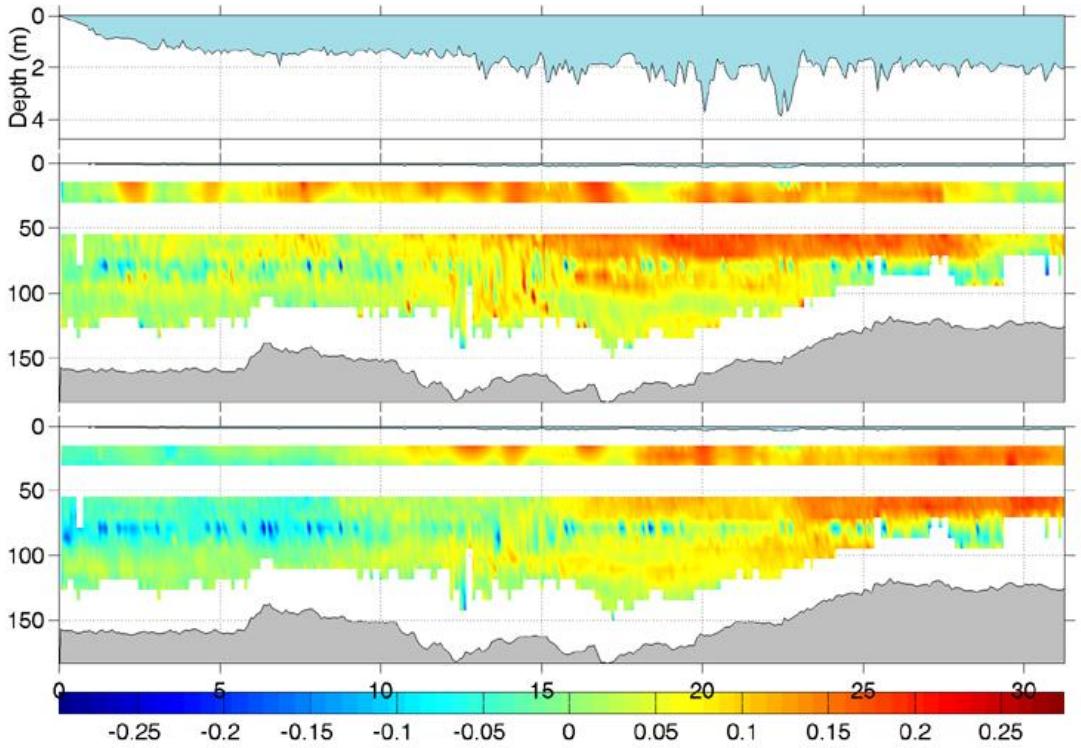

Figure 3: Outward track for mission 366. Top profile is a crude measure of ice draft, from ADCP returns. Middle graph shows N-S current velocity and bathymetry, while the bottom graph shows W-E current velocity. Horizontal scale is in km.

3. Instrument used

The Autosub autonomous underwater vehicle is one of the largest AUVs presently available, being about 7 m long, and 3.6 tonnes in weight. It has the disadvantage of requiring deckspace for two 20' containers arranged in a T-shape, since the vehicle is too long for a single container in operational mode. For our missions the Autosub was powered by 500 kg of primary manganese alkaline batteries, giving a range of over 300 km at a cruising speed of 1.8 m s^{-1}. However it should be noted that the range of the vehicle is dependent on the number of sensors being utilized as well as their sampling frequency. The depth limit for the vehicle used in this campaign was 1600 m.

The navigation system used a combination of the bottom-tracking of the Acoustic Döppler Current Profilers (ADCP) sonar system, able to track the seabed at ranges of up to 500 m, and an Ixeas-Oceano PHINS, a fibre optic gyro -based inertia navigation system (INS), which together are quoted to provide positional accuracies of 0.1% of distance travelled. In practice, the AUV returned to within 10s of metres of its target, after the runs used here, indicating significantly better performance than quoted.

The scientific payload included dual conductivity, temperature and depth (SBE-911 CTD) systems as well as dissolved oxygen sensor (SBE-43) were installed in the nose section. Upward (300kHz) and downward (150 kHz) looking RD Instruments ADCP were used for navigation, current profiling, collision avoidance and bathymetric and low resolution ice draft measurements. For high resolution mapping of the ice underside the Simrad EM-2000 swath multibeam bathymetric mapping system was mounted looking upwards. On-board storage uses off-the-shelf computer hard drives: modern drive capacities should be more than adequate for most scientific missions.

For our purposes the most important sensor on board was a Kongsberg Simrad EM2000 multibeam sonar. The EM2000 uses the so-called "Mills Cross" configuration, whereby the along-track resolution is provided by the transmitter beam pattern, and the across- track resolution is provide by the receiver array. The system transmits a 200 µs sonar pulse at 200 kHz every 1.6 s. The transmit beam is 1.5° wide in the along-track direction and insonifies a segment of total angle 120° across track (60° each side). The receive array synthesises the across-track beams with a resolution of 2.5°. The ice draft measurements are calculated from the ranges, the beam angles, the depth of the AUV and the roll, pitch and heading of the AUV. Hence the resolution and accuracy of the ice draft depend upon the depth of the AUV below the ice. At 40 m, the along- track resolution is 1 to 2 m., and across-track is about 1.8 m. Ice draft accuracy depends upon whether in-situ calibrations of zero ice thickness (e.g. leads) can be made during the survey. Where this is possible, then the single measurement accuracy is limited by system quantisation and noise, and systematic biases. Post-processing can minimise systematic differences in ice draft measurements across the track due to ray bending and differing grazing angles. We estimate overall average ice draft uncertainty as 5 cm (to one standard deviation).

The post processing of these data was carried out using MB software (an on-line freeware system designed to handle all kinds of multibeam sonar data) and displayed and archived with a uniform x- and y-pixel size of 2 m.

4. Method of analysis

We describe not only the methods used in this preliminary study but also the methods which we are seeking to develop for a more automated technique, suitable for a systematic study of a larger dataset such as that of the 2007 submarine voyage.

4.1. Location of ridges

When only one-dimensional upward sonar profiles were available, it was necessary to develop an arbitrary criterion for the identification of an individual ridge, in order to be able to generate statistics of ridge drafts, spacings and other characteristics.

Often an under-ice profile did not contain just simple well-separated triangular ridges with smooth undeformed ice in between, but instead was a jumbled mess of deformed ice. From a single 1-D profile it was impossible to tell whether such a profile represented the intersection of ridges, a single ridge with a complex structure, or an area of non-linear deformation consisting of individual deformed ice blocks. Therefore, to obtain statistical information from such profiles, the arbitrary definition was developed (Wadhams, 2000), that *an independent ridge must have a crest draft relative to the local undeformed ice which is more than double that of the troughs which bracket it.* This is akin to the Rayleigh criterion for separating spectral lines. In the case of 1-D profiles an arbitrary draft of 2.5 m was specified for the undeformed ice, but in the case of 3-D profiles it is easier for us to recognize the nearest undeformed ice and obtain more accurate values for its draft.

In an automated system we will use this criterion to flag individual pressure ridges, each of which will be analysed. In the present preliminary study of 9 well-defined ridges we were able to recognize and separate them from their neighbors by eye. The Rayleigh criterion will be operated along the y-axis (assume that the y-axis is the axis of motion of the vehicle, x- is the cross-track axis with x=0 at centreline, negative values to port when measured along the axis of motion, and positive values to starboard).

4.2. Method of locating a crest

Define a “starter baseline” as a line across the track (y = 0) covering undeformed ice just before the ridge is encountered. Starting from x = -W/2, where W is the width of the swath, move along the y-axis from the starter baseline until the ridge crest (point of maximum draft) is reached. Continue until ridge end point is reached, an “end baseline” beyond the ridge structure. Find standard deviation of this stretch of profile. Record all pixels occurring between the crest and the crest minus one standard deviation in height. Continue with next line of pixels at x = -W/2 +2 (pixels are 2 m wide) and repeat. Continue to x = +W/2. Result is a swath in which the crest is flanked by points of lower draft.

Find the linear or curved regression line which best fits all the points on the swath. It will run along the ridge crest, but will not exactly reproduce it. This technique deals with the effect of random blocks which can give a false position for the crest.

Two possible approaches will be tested: (1) Giving all points equal weight, (2) Weighting points by their depths, so that the actual wiggly or random line of the crest is modulated to a lesser extent by the pixels of lower draft. In this study we have used approach (1), but we recognise that sometimes this leads to unnecessary offset of the defined crest from the real crest, and so we will change to a weighted function for the automated technique. Also, the nine ridges chosen for the preliminary study all had crests which could be represented by a linear function.

4.3. Finding cross-sections for a ridge

Having identified the straight or curved line of the ridge crest, we move along it at 4 m (2 pixel) increments and draw a section at right angles to the local line of the crest. We continue until the full width of swath has been sampled. If ridge was linear, these sections will be parallel. If curved, they will have different orientations.

We draw the cross-sections as far as a standard end-point (possibly half crest depth) and consider two parts to each section z = f(d). Firstly, from the start point to the crest, then from the crest to the end point. We determine first whether the shape is closer to a **triangle** or a **trapezium**.

If a triangle, determine mean **slope angle** of each face by linear regression.

If a trapezium, use optimisation analysis to find best fit to **slope angle of each face, depth and width of flat bottom.**

Slope angles are calculated independently for both sides of the ridge slice. The programme identifies a level ice thickness as the root-mean-square (RMS) value of contiguous points of less than a specified Level Ice Draft (LID, currently manually tuned, more sophisticated determination necessary for an automated system). The ridge is detected when draft exceeds one standard deviation of this RMS value. Slope angle is calculated as the best fit straight line between this point and the maximum draft value, which is assumed to divide the ridge.

If insufficient level ice is found (<6 points conforming to the above criteria), then a Rayleigh limit (half maximum draft) is used to define the slope. If drafts are all greater than the Rayleigh limit, then the minimum draft on that side is used. A draft minimum (point of inflection) is selected if this forms an obvious delineation of the ridge and is less than the Rayleigh draft.

We also calculate the "volume equivalent slope", which conserves volume across the slice, variously using the level ice draft, the Rayleigh value or minimum draft as the base value, as appropriate. This volume equivalent slope is of more relevance to mechanical force calculations, as it accounts for the total mass of ice involved. The angle is often greater than for the regression result, since it is constrained to begin from a specified base level, which in reality is often followed by a marked step in draft.

Finally, we calculate a mean slope, weighted by the slant length of the slope in question, i.e.:

$$\bar{\theta} = \frac{\sum \theta_i . w_i}{\sum w_i}$$

where θ_i and w_i are the slope angle and slant length, respectively, of the individual slice *i*.

The same analysis is then performed for the **overall mean shape of all the cross-sections**. The overall shape is determined by aligning all the sections to their

point of maximum draft (the ridge crest), and then taking the median of all drafts in 2m (one pixel) bins from the crest.

Individual cross-sections are used to determine standard deviation for slope angle and crest draft parameters for any given ridge (see Table 1, page 18).

4.4. Composite ridges

Determine the envelope of the along-crest shape of the ridge by considering H = f(x) where H is crest height at swath x. Generate along-crest variability statistics. These will include a 20 m running mean. If running mean deviates by more than 50% along swath, it indicates that the ridge is composite, i.e. is made of two or more sections which have suffered different degrees of deformation. Treat these separately in the analyses. This did not apply to any of the 9 ridges used here.

4.5. Tests of ridge age

It is our intention (in Phase 2) to develop an automatic analysis which will ascribe FY or MY categories to each ridge. In Phase 1 we have performed preliminary tests. These include the following.

a) If ridge shape is triangular, look at vertical deviations of profile of ridge from pure triangle. Determine along-profile statistics such as autocorrelation function, rms deviation, meander coefficient.

b) Ditto if best fit is trapezium.

It is possible to be sure that some ridges are FY because the nearest undeformed ice on either side of the crest has characteristic thickness of FY ice (about 1.5 m). However, it is harder to identify MY ridges because an FY ridge can exist in MY ice, and there is an even greater ambiguity if a ridge exists between FY and MY undeformed ice. Having surveyed several ridges, we will be able to see if sets of parameters of the small-scale deviations fit into two well-separated clusters, one of which can be identified with definite FY ridges. If so, we will have found our method for differentiating between FY and MY ridges.

5. Description of ridges used in preliminary study

For the preliminary analysis we chose nine well-defined ridges from runs 365 and 366 of Autosub. Their locations and general descriptions are are discussed here, with a 3D perspective view of each. Mean cross sections and slope angles are given in the next section, detailed tables of slope parameters for each slice are given in Appendix A.

We note that the sample of ridges selected for this study contains only 2 MY ridges and 7 FY ridges (including one shear ridge and 2 possible cases of rafting). Except for ridge 1, the ridge drafts are also rather small. For this first study we were seeking isolated and very well-defined ridges, in order to develop and test the algorithms for deriving ridge shapes. Such ridges tend to be first-year, as we have found from our AUV and submarine experiments that multi-year ice often contains deformation features which are not linear but almost like random pinnacles; these pose more of a challenge for analysis and we wanted to test the algorithms first on “classic” linear pressure ridges.

Ridge 1

Ridge 1 was the deepest ridge encountered during mission 365, marked A in fig. 2. It is 33 m deep, and represents a formidable mass of ice (the slice visible in the figure weighs about 200,000 tons). Since the individual ice blocks which compose ridges are quite small, the ridge itself is a relatively uniform triangle in cross-section, representing the angle of repose of a pile of buoyant ice. Wadhams (1978b) drew attention to this characteristic of ridges deeper than 30 m in an analysis of submarine profiles. A lesser ridge is visible in the foreground. The undeformed ice on either side of the ridge is about 4 m in draft, i.e. formidable multi-year ice, and so we conclude that this is most likely an **MY ridge**. It is basically triangular in cross-section though with some flattening off at the crest. Only a 40 m wide swath of the image was usable for the analysis, since the great depth of the ridge relative to the AUV's depth caused some distortion and drop-outs of the outer parts of the beam.

Figure 4: Perspective view of Ridge 1

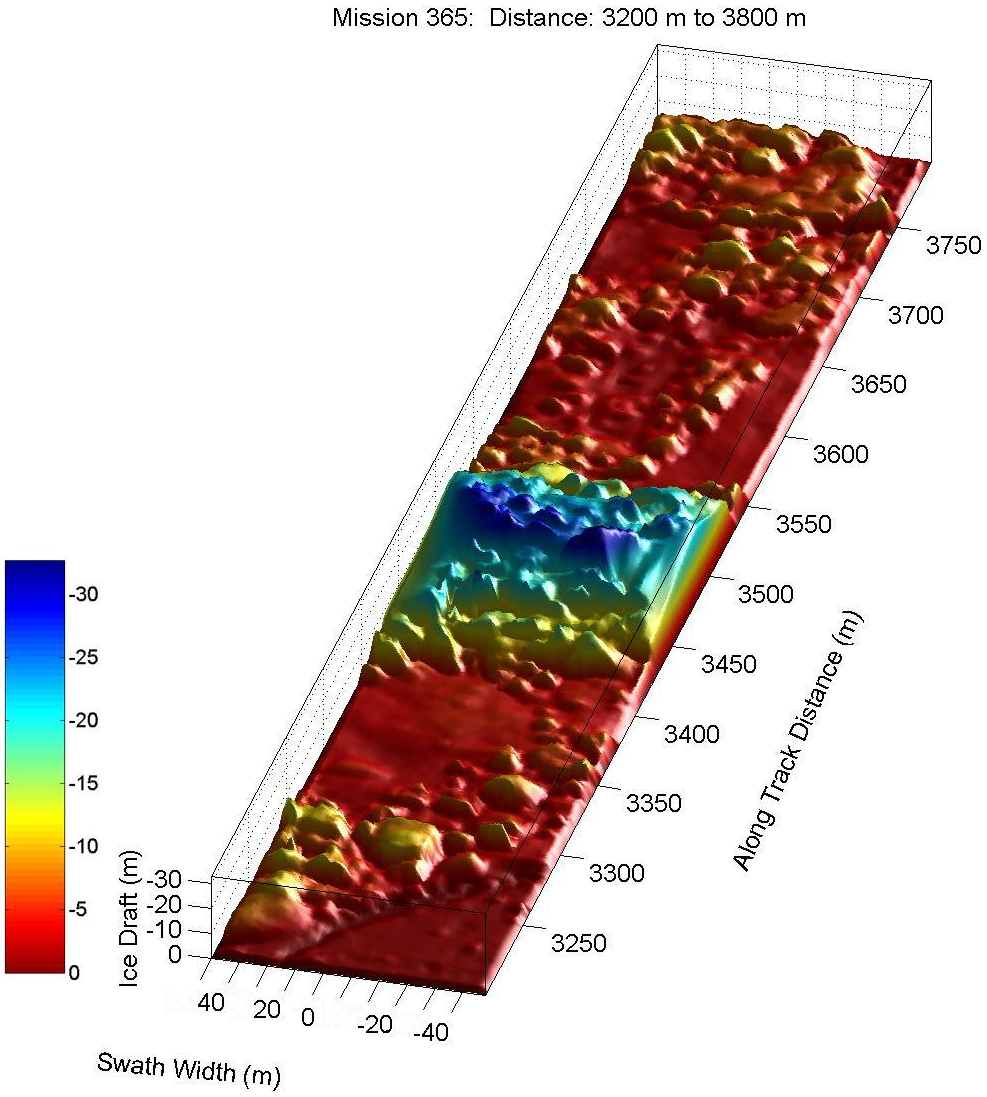

Ridge 2

Ridge 2 occurred 17 km to the west of the start point of mission 365. It has a somewhat meandering, but basically linearly-trending crest line, and is clearly an **FY ridge**, since the undeformed ice on one side of it has a draft of 1.1 m and on the other about 1.7 m. It is quite a shallow ridge with a draft of only 4.5 m, but it is well defined as having a linear ridge-like shape.

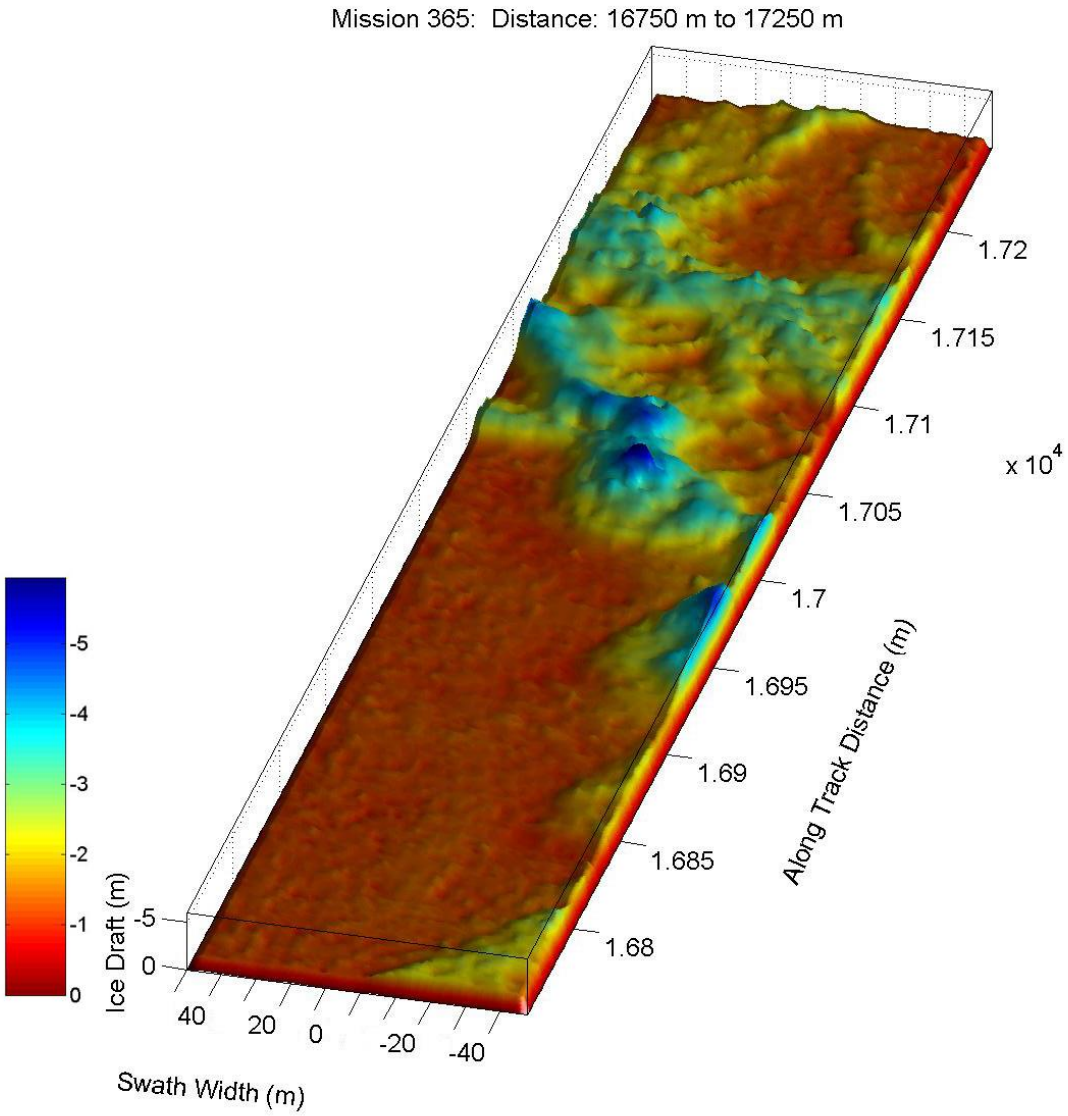

Figure 5: Perspective view of Ridge 2

Ridge 3

Ridge 3 occurred 17.7 km along the track, i.e. only 0.7 km west of ridge 2. It resembles ridge 2 in having a meander superimposed on a linearly-trending crest line, on being shallow (4 m or less) but well defined, and being surrounded by first year ice of draft 1-2 m. This again is an **FY ridge.** It is oriented in an along-track sense so that 200 m of the ridge crest are visible in the swath and are available for analysis.

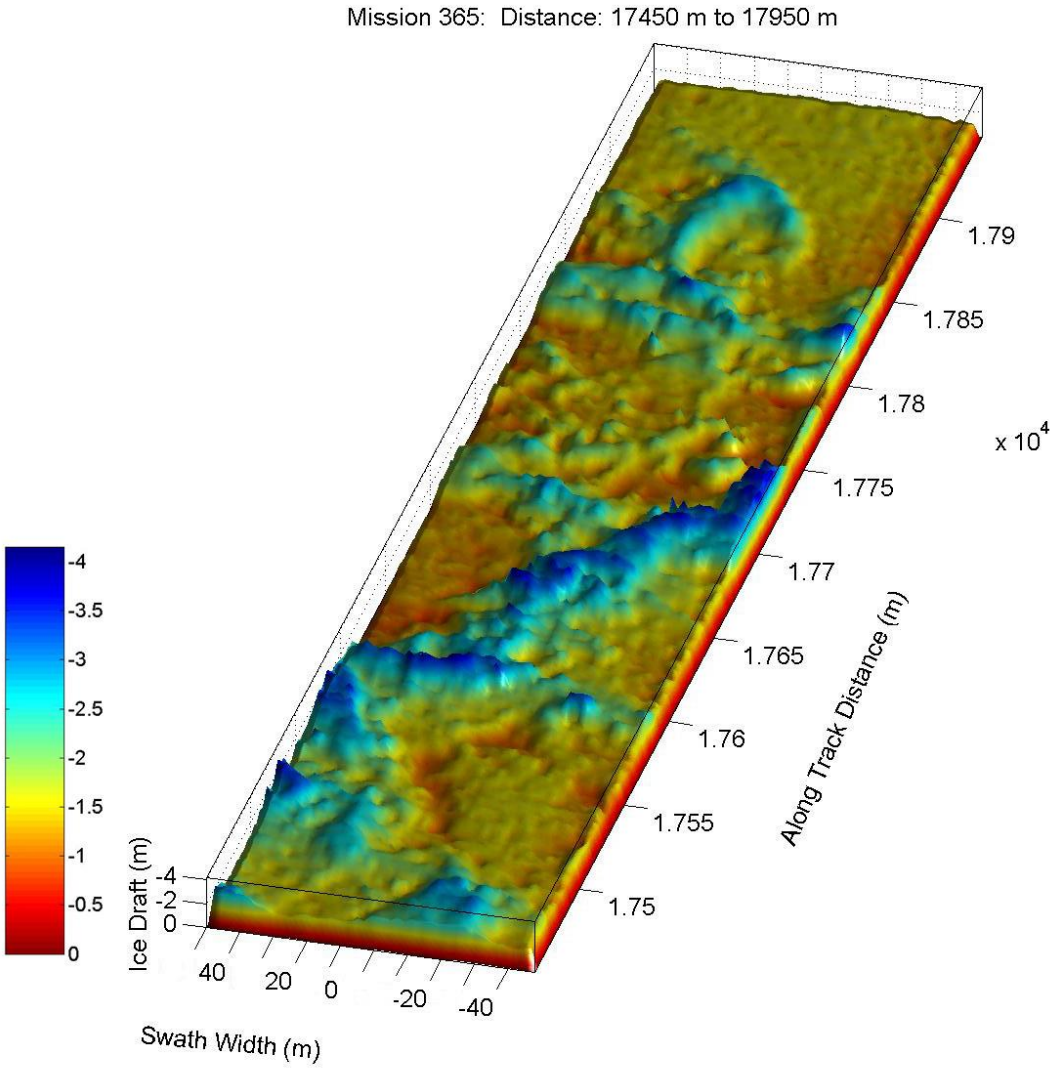

Figure 6: Perspective view of Ridge 3

Ridge 4

Ridge 4 occurred 24.8 km along the mission 366 track. It is less narrowly linear than ridges 2 and 3, and broadens into a large block on the right-hand side. Although the ridge draft is only 6 m the ice on either side is quite thick. At the top there is undeformed ice 2 m thick, which is a thickness that is somewhat high for first-year ice though low for multi-year – it may be second-year ice. At the bottom there is a more undulating ice cover of 2 – 3.2 m thickness, which looks like MY ice. The age of this ridge is therefore difficult to determine, although we suspect **MY.** This is a case of a ridge where the examination of secondary characteristics (e.g. small scale roughness) may be needed to assign an age, as mentioned in section 4.5.

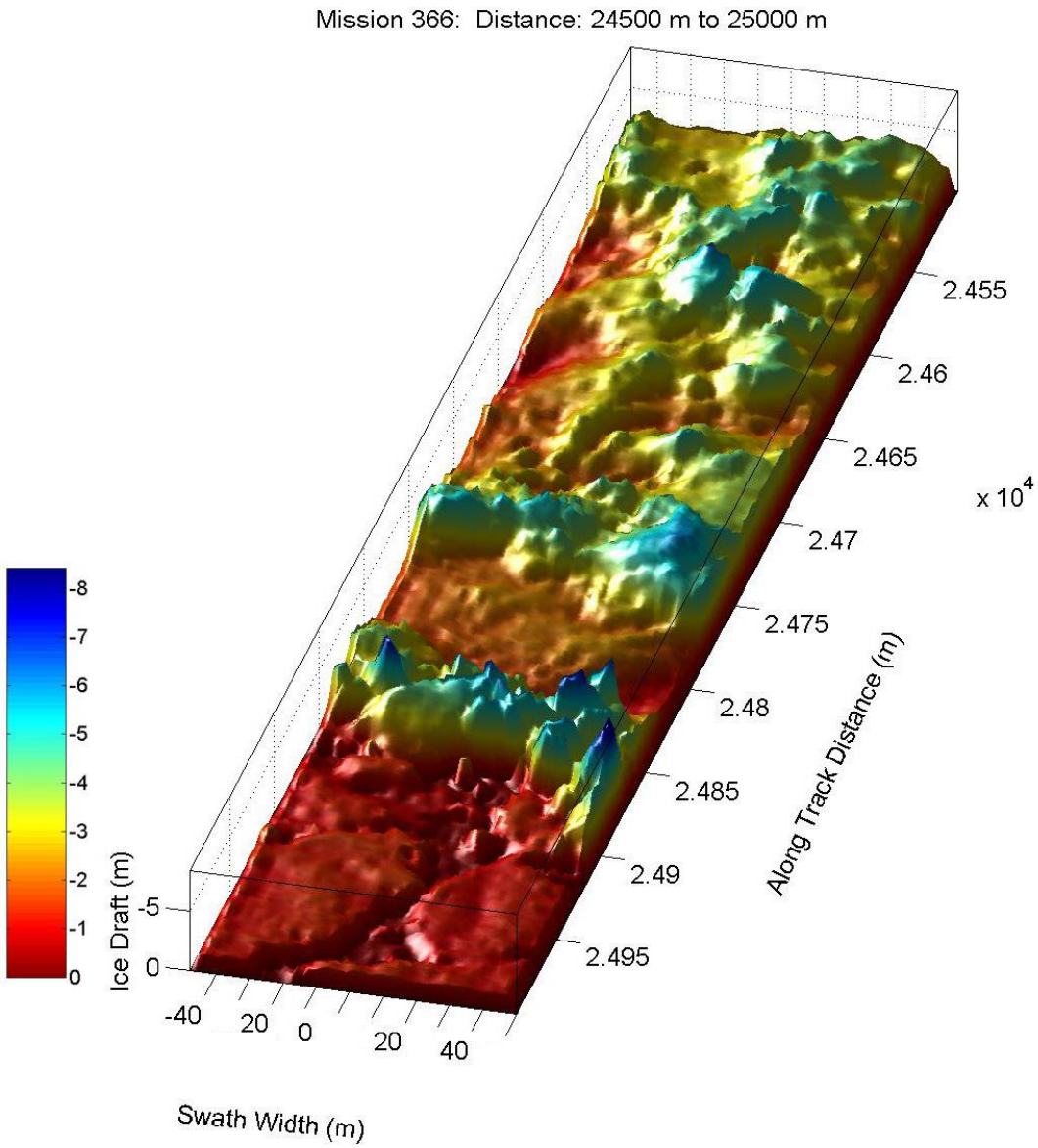

Figure 7: Perspective view of Ridge 4

Ridge 5

Ridge 5 occurred 28.7 km along the track of mission 366. It is a very clear case of a small **FY ridge.** Draft is only 3 m, while it is surrounded by uniform ice of draft 1.3 – 1.5 m, typical of first-year ice. It is a linear ridge, very narrow and with a perfectly triangular cross-section. The draft of the ridge being about double the thickness of the surrounding ice, it is tempting to suppose that this is a case of rafting rather than ridging**,** with a compressive stress causing ice to ride up along the edge of a recently-opened linear crack, making a two-layer "sandwich". The triangular shape of the ridge, however, tells against this.

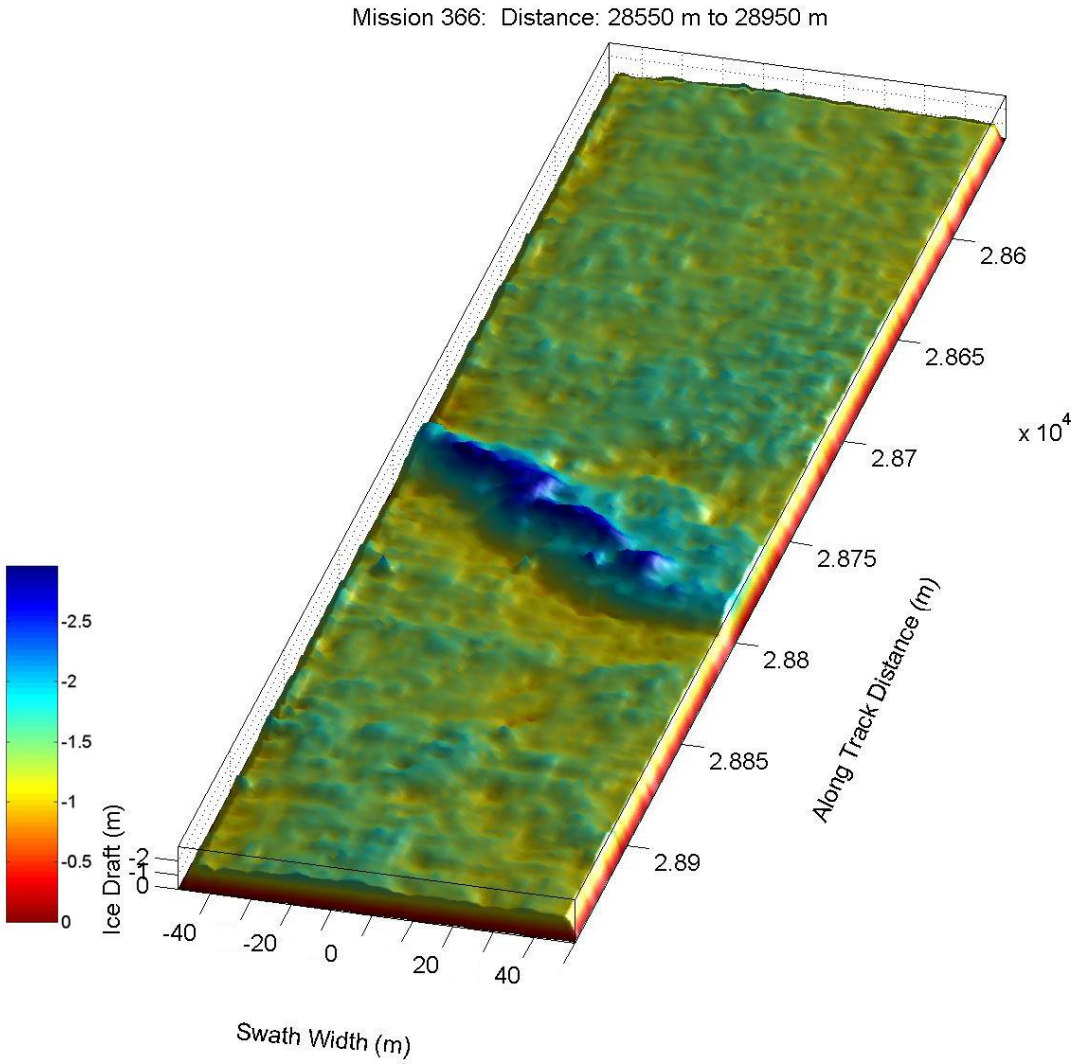

Figure 8: Perspective view of Ridge 5

Ridge 6

Ridge 6 occurred 65.3 km along the track of mission 365, i.e. far to the west of Belgica Bank and close to the coast of Greenland (it is ridge B in fig. 2). It is probably a shear ridge of some 6 m draft in a wide expanse of uniform fast ice. Probably it formed when wind stress caused a long crack to form in the fast ice sheet overlying Norske Trough, then the more mobile side of the sheet (probably on the east side, the west side being fast to the nearby Greenland coastline) was sheared against the other side of the crack, building up a ridge out of small ice blocks. The ridge appears to contain a "fracture zone", a place where the line of the ridge makes a jog to the west, just like a fracture zone in a mid-ocean ridge. The ridge axis is oriented at 45° to the track of the AUV. The fast ice around the ridge has 1.7 m draft, while further to the east, across the trough and bank, it is only 1.0-1.3 m, indicating either that in this western part of Norske Trough, close to the continental influence of Greenland, the ice grows more rapidly, or that unbalanced isostasy in the ridge is affecting the draft of nearby ice. The thicknesses are characteristic of **FY ice**. The ridge itself is only 5.5 m in draft, but slopes away much more gently than other ridges in this study.

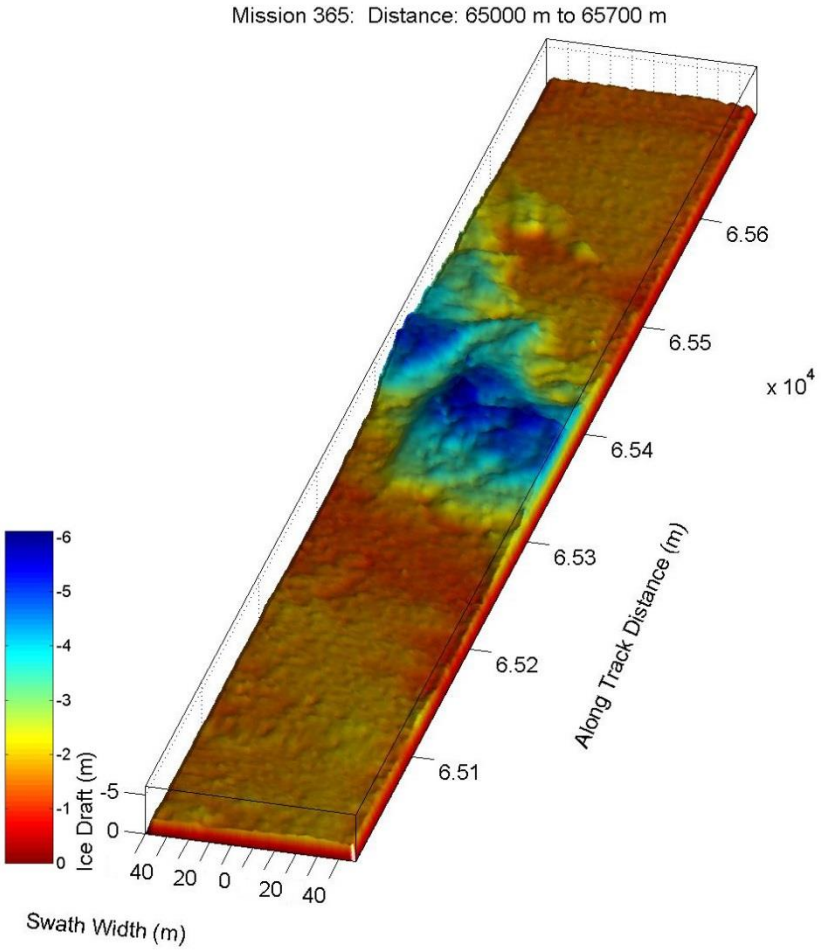

Figure 9: Perspective view of Ridge 6

Ridge 7

Ridge 7 was 104.1 km along-track in mission 365, which implies that it was recorded on the vehicle's way home. It is a very well-defined narrow FY ridge, only 2.4 m in draft. The surrounding ice is 0.9 m – 1.1 m in draft, implying not only **FY** ice but ice which started to grow later in the winter, perhaps from an open lead. Again there is the possibility that it is a rafting feature.

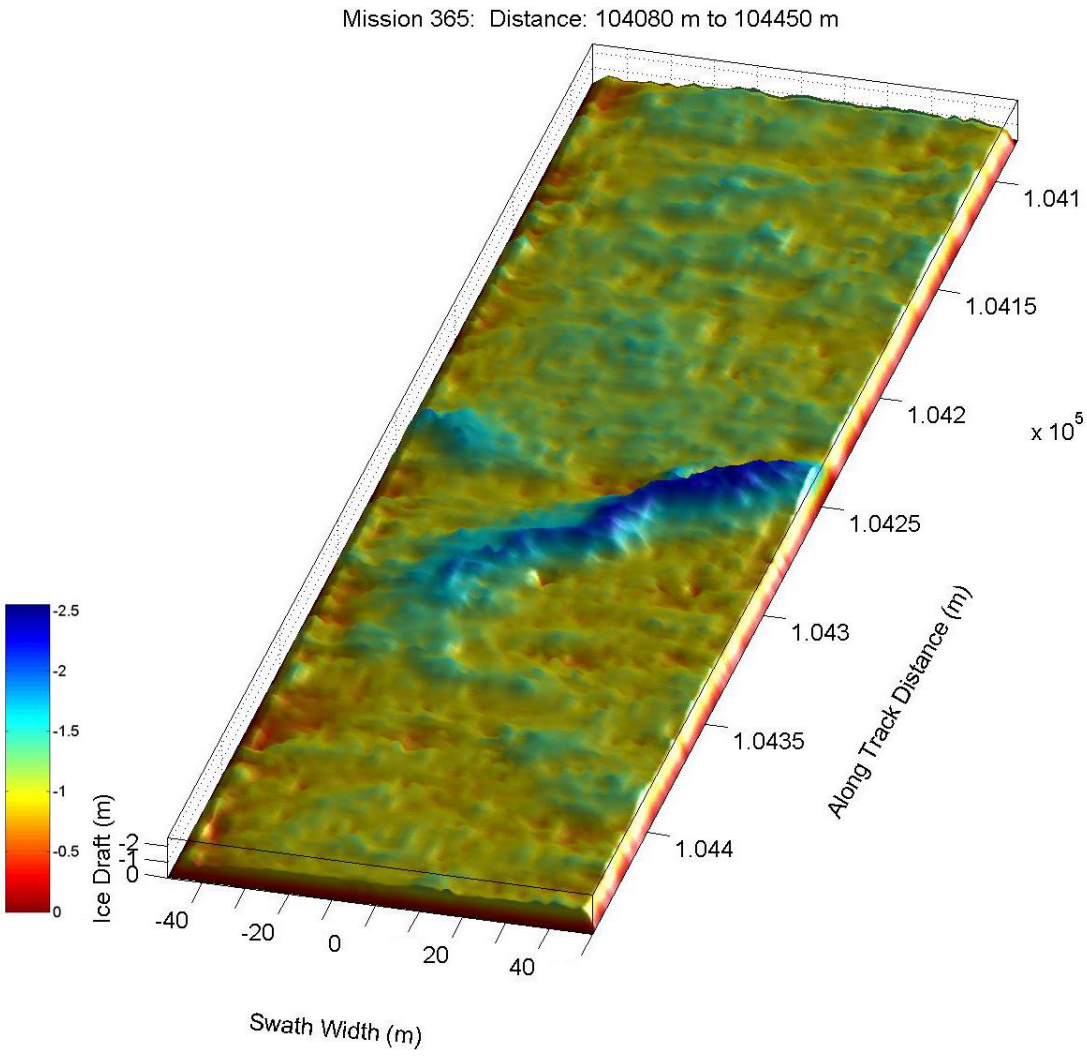

Figure 10: Perspective view of Ridge 7

Ridge 8

Ridge 8 was 135.7 km along-track on 365, again implying the homeward leg. It is another well-defined **FY ridge**. The ridge crest appears to curve towards the right hand side but we have approximated it by a linear regression. The undeformed ice on either side is 1.3 – 1.6 m in draft, i.e. well-developed first-year ice, while the ridge is a steep triangle extending down only to 3.5-4 m.

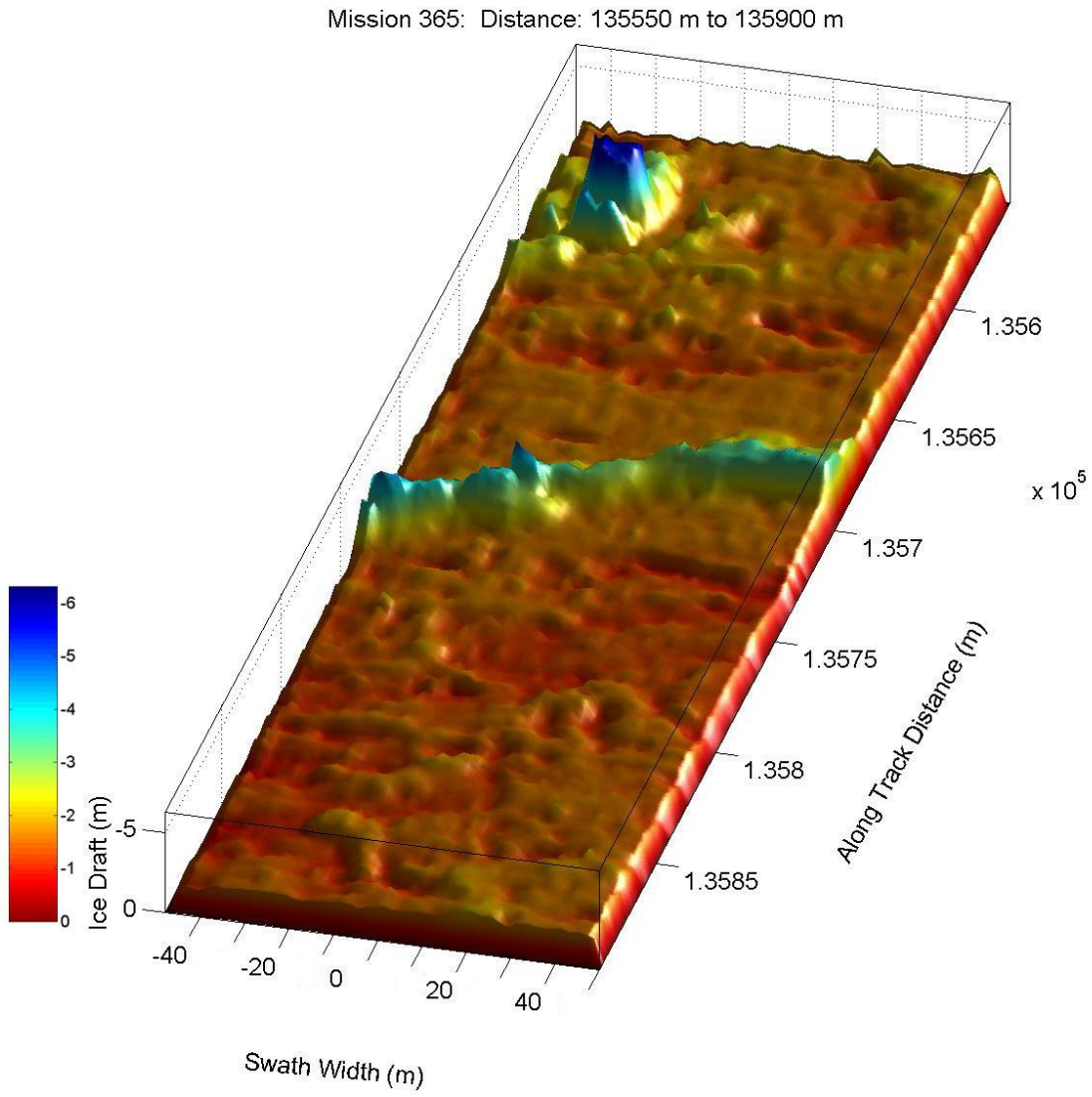

Figure 11: Perspective view of Ridge 8

Ridge 9

Ridge 9 was 23.3 km along the track of mission 365. It broadens out from a narrow shallow ridge to a large smooth block 5 m deep on the right hand side of the swath. Surrounding ice is only 1 m thick, so this is an **FY ridge.** Nevertheless its structure is odd, since the existence of large semi-isolated smooth blocks within the structure of a ridge is something which we have noticed in close-up studies by the Gavia AUV in 2007 and 2008 to be a defining characteristic of multi-year ridges.

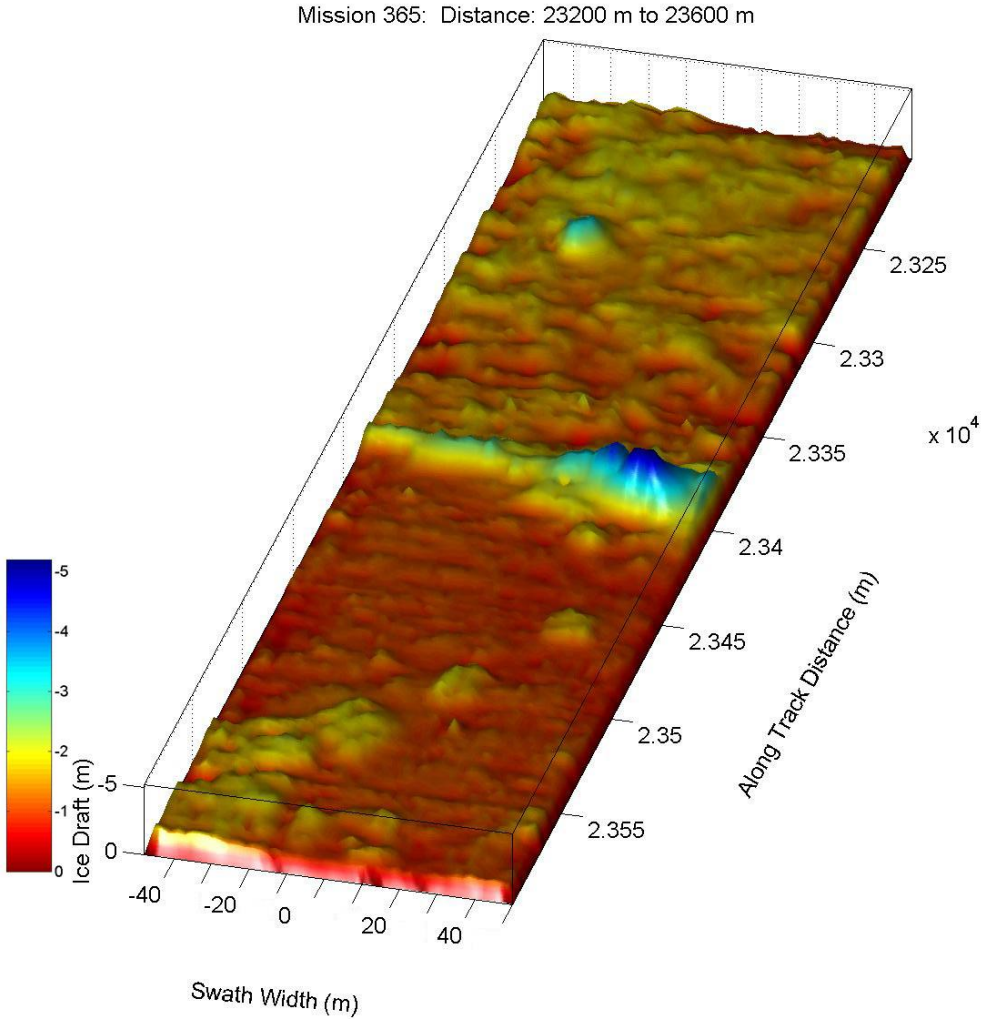

Figure 12: Perspective view of Ridge 9

6. Results of ridge structure analyses

The mean shape of each ridge, together with its analysed slopes are shown in Figure 13 (a) to (i), on the following three pages. Individual cross-sections, or slices, are plotted in light blue, with the median cross-section in dark blue. Analysed slopes are marked in magenta (linear regression result) and red (volume equivalent result). The base level for the volume equivalent slope is marked as a dashed horizontal black line. The limit of the ridge on both sides is marked by a vertical solid black line.

The same analysis was performed on each slice individually, and these detailed tables are included as Appendix A. Slopes from these slices were used to calculate the Standard Deviation results in Table 1, below. The Standard Deviation measure, though requested, does not give a good picture of the slope variability, since most outliers (high values) occur for very small ridge slant lengths and therefore do not affect the median or weighted overall slope angle significantly.

Table 1: Summary of ridge parameters. ϕ - angle of ridge crest relative to AUV track (90° indicates the AUV crosses the ridge perpendicularly); D_{max} – maximum draft ± the standard deviation of max draft along the ridge; L – length of ridge crest in sonar swath; W – horizontal extent of ridges (distance between vertical lines in Fig. 13); θ - slope angle of ridge (LHS/RHS); θ_{Veq} – 'volume equivalent' slope angle, LHS/RHS. Standard deviations for LHS and RHS slopes are also given for both angle calculation methods.

Ridge #	ϕ	$D_{max} \pm STD$, m	L, m	W, m	$\theta \pm$ SD, L/R	$\theta_{Veq} \pm$ SD, L/R
1	83°	32.70 ± 2.29	34.38*	125.62	16°/20° ± 8/2	28°/20° ± 4/3
2	39°	6.03 ± 0.41	116.71	54.34	6°/5° ± 5/6	5°/4° ± 5/5
3	30°	4.20 ± 0.50	180.39	67.51	3°/4° ± 4/4	3°/3° ± 4/4
4	76°	6.12 ± 0.68	92.79	65.02	7°/4° ± 3/2	7°/3° ± 3/3
5	56°	3.04 ± 0.36	109.15	53.89	2°/4° ± 2/1	1°/4° ± 2/2
6	51°	6.14 ± 0.62	116.09	165.35	3°/3° ± 1/1	3°/3° ± 1/1
7	47°	2.43 ± 0.21	96.48	34.03	4°/4° ± 3/1	3°/4° ± 4/1
8	65°	4.73 ± 0.49	99.53	30.17	7°/9° ± 4/3	6°/9° ± 5/3
9	81°	5.23 ± 0.88	91.15	26.58	6°/6° ± 4/4	6°/7° ± 5/5

* limited ridge length due to the sonar being close to the bottom of the ridge, hence limited coverage

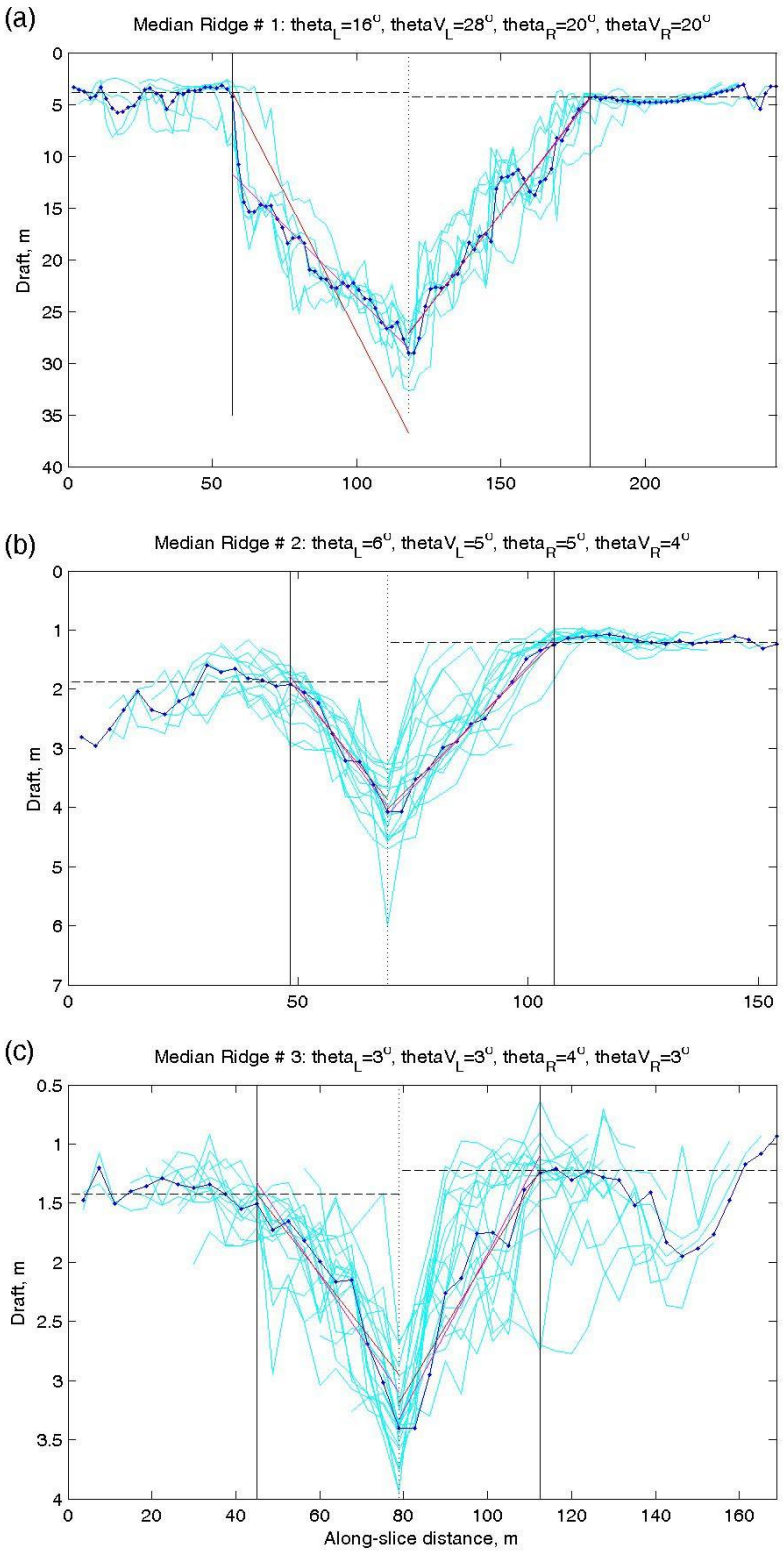

Figure 13 (a)-(i): Median shapes of the nine ridges (dark blue), with individual slices marked in light blue. Also shown are the calculated slopes, using linear regression (magenta) and equivalent volume (red) methods. Vertical solid black lines delineate the detected ridge width. Dashed horizontal lines show the corresponding draft on each side.

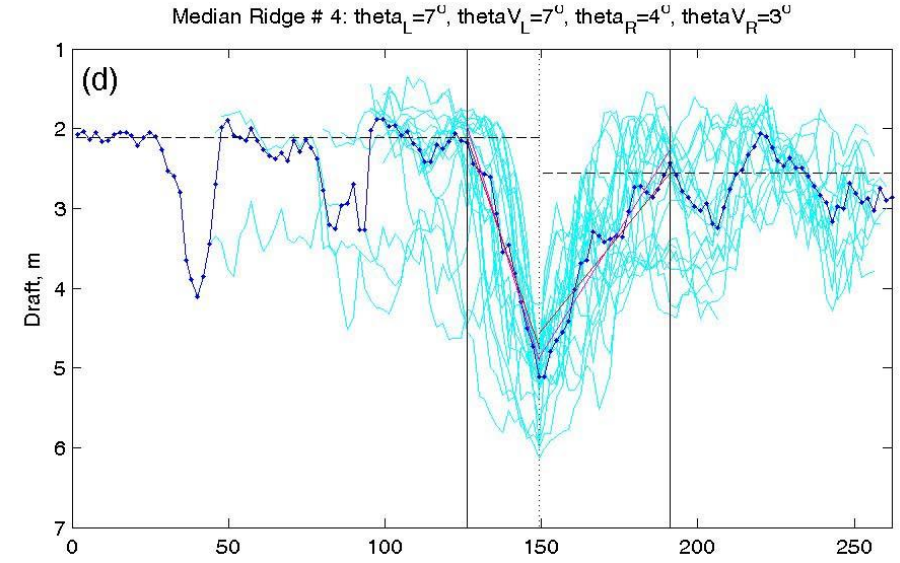
Median Ridge # 4: theta$_L$=7°, thetaV$_L$=7°, theta$_R$=4°, thetaV$_R$=3°
(d)
Draft, m
1
2
3
4
5
6
7
0
50
100
150
200
250

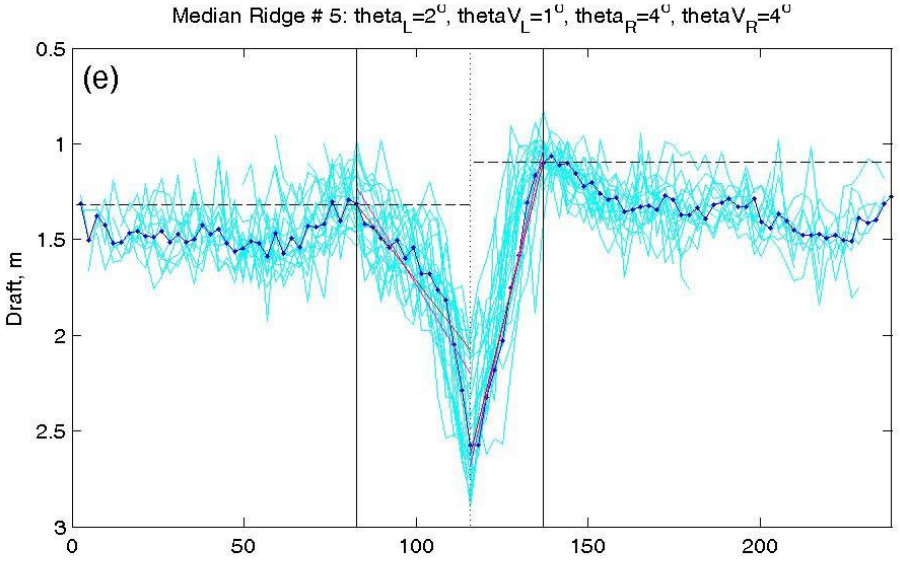
Median Ridge # 5: theta$_L$=2°, thetaV$_L$=1°, theta$_R$=4°, thetaV$_R$=4°
(e)
Draft, m
0.5
1
1.5
2
2.5
3
0
50
100
150
200

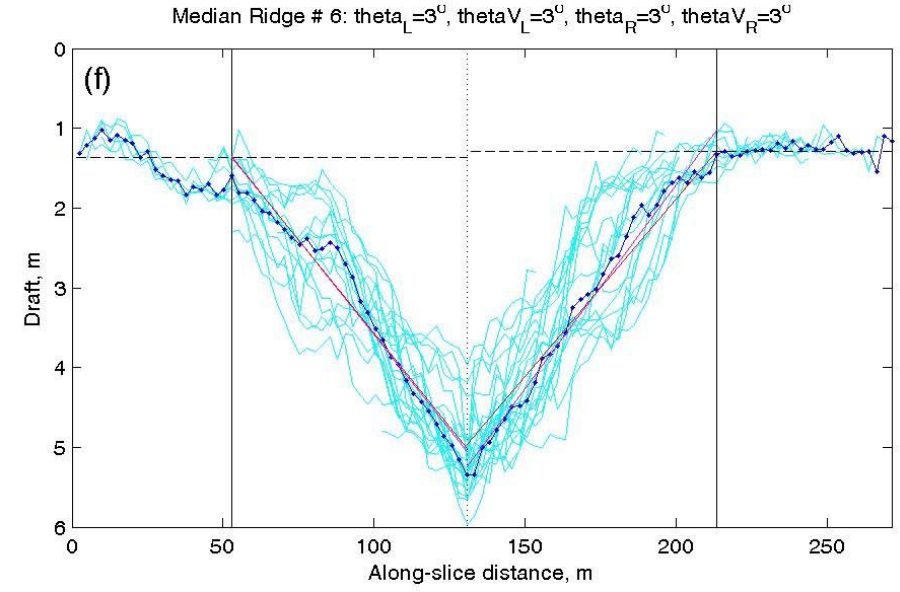
Median Ridge # 6: theta$_L$=3°, thetaV$_L$=3°, theta$_R$=3°, thetaV$_R$=3°
(f)
Draft, m
0
1
2
3
4
5
6
0
50
100
150
200
250
Along-slice distance, m

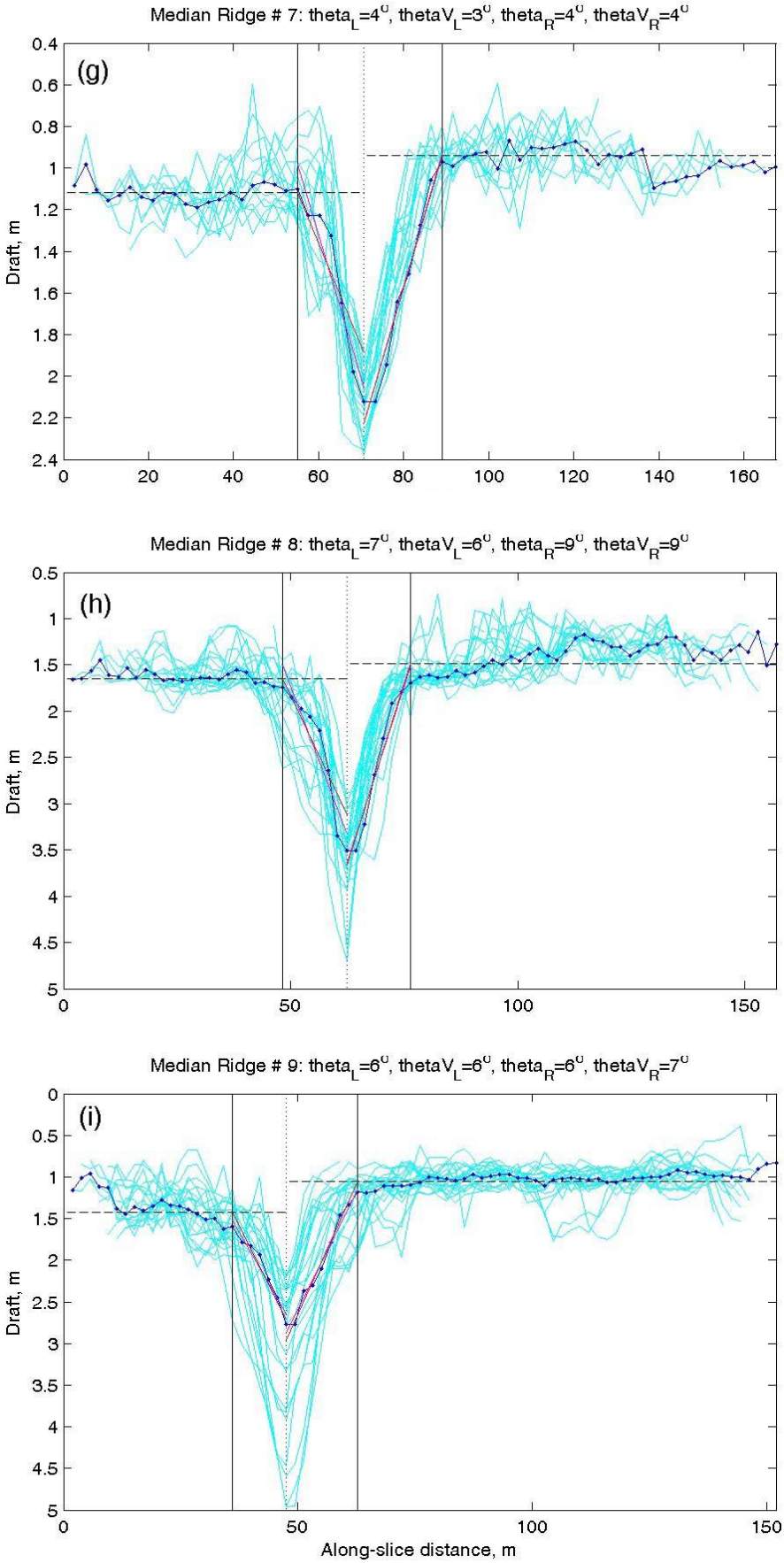
Median Ridge # 7: theta$_L$=4°, thetaV$_L$=3°, theta$_R$=4°, thetaV$_R$=4°
(g)
Median Ridge # 8: theta$_L$=7°, thetaV$_L$=6°, theta$_R$=9°, thetaV$_R$=9°
(h)
Median Ridge # 9: theta$_L$=6°, thetaV$_L$=6°, theta$_R$=6°, thetaV$_R$=7°
(i)
Draft, m
Along-slice distance, m

7. Conclusions.

Ridge data

Of the nine ridges, ridge 1 is the only one that fits previous analyses of ridge slopes. It is also by far the deepest ridge. In the study of 729 ridges by Davis and Wadhams (1995), all of them corrected for orientation by the use of sidescan sonar, the mean ridge slope was 21.7º - 26.5º (depending on region), although the overall range was 4º to 64º. The modal slope for the regions which lay N and E of Greenland was 18º. The observed slope of 16º/20º (or 20º/28º on another definition) therefore lies well within the typical values obtained in that study. The study employed a cut-off of 5 m for ridge draft, with a further bias towards deeper ridges set by the fact that ridges had to be prominent enough to be detectable both by the upward and the sidescan sonar. The mean drafts of the ridges studied were 7.5 – 11.8 m (modes 6 – 9 m), which meant that most ridges were deeper than ridges 2-9 but shallower than ridge 1.

With respect to ridge 1, an earlier study by Wadhams (1978b) is even more relevant because this dealt only with ridges deeper than 30 m in a 1976 submarine transect. Wadhams found 45 such ridges, and obtained average slopes by the probabilistic assumption of random orientations relative to submarine track. The resulting slope distribution was peaked in the range 16º-28º with an overall mean of 23.9º, again showing that ridge 1 is very typical of deep Arctic MY ridges.

Ridges 2-9 appear to be quite anomalous with respect to these results. Although each ridge had a well-defined triangular ridge-like shape, as shown in the above composite profiles, and although the ridges appeared as well-defined linear ridge-like features in the 3-D plots, we find that the slope angles are very gentle, only 2º – 9º. This is quite extraordinary, and applies to the MY ridge 4 as well as the seven FY ridges. The 2007 study of a single recently-formed FY ridge by AUV (Wadhams and Doble, 2008) showed the ridge as being made up of small ice blocks which gave the ridge a steep-sided profile. Similarly, earlier studies where many FY ridges were drilled (e.g. Kovacs, 1972) always show mean slopes that are, if anything, greater than those of MY ridges (Kovacs found a mean of 33º), allowing us to conclude that years of current flow over a ridge cause it to mature into a hummock with a more gentle slope. We therefore find ridges 2-9 of some interest.

Two possible hypotheses are:-

1. These are not ridges at all but rafted ice. Weeks et al. (1971) showed that if a linear crack opens and the floes on either side are pushed together before significant refreezing occurs, then the mode of deformation is often rafting rather than ridging for parent floe thicknesses of less than 1 m. It is conceivable that each of these apparent ridges is offering a misleading appearance, that the “crest” is simply the bottom edge of the floe that was rafted under the other, while the “slopes” are the slope angles adopted by the ice near the rafting site to retain isostatic balance.
2. There is a class of shallow ridge, perhaps made up of only a few blocks of refrozen lead ice, which do have very shallow slopes. These would have fallen through the net of previous analyses, which usually employed a cut-off of 5 m when dealing with upward-looking sonar data alone.

Although of interest from the point of view of ice mechanics, these shallow ridges are clearly not important in considering extreme values and design loads. Their chief value was in providing appropriate shapes for testing the developing algorithms for automated ridge analysis.

Under-ice operations

Autosub operated very successfully under Arctic sea ice, obtaining 458 km of high quality upward looking swath sonar data and accompanying oceanographic data. It undertook necessary avoidance manoeuvres for obstacles, and the acoustic homing system ensured that the vehicle could be returned with confidence to an area covered with loose moving pack ice. The vehicle is clearly a rugged and useful measuring tool for studies under sea ice. The combination of an unmanned under-ice vehicle and a multibeam sonar gives, literally, a new dimension to under-ice studies, and is important for work on ice thickness change, the disappearance of deep ridges from the Arctic, navigability in ice, the effects of oil and other pollutants, the interactions between sea ice and under-ice currents and water structure, the underside as biological habitat, and other studies critical to the role of ice in polar climate change.

Two strategies for under-ice mapping using 3-D sonar are developing: *local studies* using an AUV under a specific structure such as a single ridge, a ridge system, a rubble field or an iceberg, to obtain a gridded map of the whole feature; and *synoptic studies* using a submarine or a long-range AUV to yield a large enough sample of the Arctic pack ice to be capable of generating large-scale statistics on ridge geometries. The present study is a start towards setting up an analytical structure for synoptic 3-D under-ice data.

It is clear from the present study that, if we are interested in ridges of all depths, a large sample is needed to obtain statistically meaningful conclusions about slope angles, even with the added precision and reliability provided by 3-D data, because of the high variability and anomalous behaviour of shallow ridges. The analysis of longer stretches of multibeam data is necessary; at present the only such dataset is that obtained in 2007 by HMS *Tireless.* The fit of the single very deep MY ridge to previously analysed data shows, however, that a much smaller number of very deep ridges may provide reliable information about their typical shapes. The problem, of course, is that a long transect is required to generate enough very deep ridges for such a study, but one could speed up the process by screening the profile and not considering ridges shallower than a cut-off of, say, 10 m. The strategy to pursue naturally depends on the aims of the analyst: a study of the design load due to extreme ridges could focus on the deeper ridges only, while a study which seeks to understand the role of ridging in ice dynamics/thermodynamics would need to consider shallower ridges as well.

References

Böhm, E., T.S. Hopkins and P.J. Minnett (1997) Passive microwave observations of the Northeast Water Polynya: 1978-1994. *J. Mar. Sys.,* **10***,* 85-94.

Bourke, R.H., J.L. Newton, R.G. Paquette and M.D. Tunnicliffe, (1987). Circulation and water masses of the East Greenland Shelf. *J. Geophys. Res***., 92,** 6729-6740.

Davis, N.R. and P. Wadhams (1995). A statistical analysis of Arctic pressure ridge morphology. *J. Geophys Res.*, **100***(*C6), 10915-10925.

Doble, M.J., Forrest, A.L., Wadhams, P. and B.E. Laval (2008). Through-ice AUV deployment: operational and technical experience from two seasons of Arctic fieldwork. *Cold Reg. Sci & Tech*. doi: 10.1016/j.coldregions.2008.11.006

Higgins, A.K., (1991) North Greenland glacier velocities and calf ice production. *Polarforsch.* 60, 1–23.

Hirche, H-J. and J.W. Deming (eds) (1997). Northeast Water Polynya Symposium. *J.*

Mar. Sys., 10(1-4).

Jakobsson, M., N. Cherkis, J. Woodward, R. Macnab and B. Coakley (2000). New grid of Arctic bathymetry aids scientists and mapmakers, *EOS Trans. Am. Geophys. U*., *81***,** 89, 93, 96,

See also http://www.ngdc.noaa.gov/mgg/bathymetry/arctic/arctic.html.

Kovacs, A. (1972). On pressured sea ice. In *Proc. Intl. Sea Ice Conf., Reykjavik* (ed. T. Karlsson). Nat. Res. Counc. Iceland, Reykjavik, 276-295.

Mohr, J.J. and R. Forsberg (2001). Searching for new islands in sea ice. *Nature***, 416***,* 351.

Reeh, N,.C., H.H. Thomsen, A.K. Higgins and A. Weidick (2001). Sea ice and the stability of north and northeast Greenland floating glaciers. *Ann. Glaciol***., 33,** 474-480.

Wadhams, P. (1978) Sidescan sonar imagery of sea ice in the Arctic Ocean. *Can. J. Remote Sensing,* **4**(2), 161-173.

Wadhams, P. (1978b) Characteristics of deep pressure ridges in the Arctic Ocean. *Proc. 4th Intl. Conf. on Port & Ocean Engng Under Arctic Condns*., St. John's, 26-30 Sept. 1977 (ed. D. B. Muggeridge). Memorial Univ. of Nfld., St. John's, *1*, 544-555.

Wadhams, P. (1983) The prediction of extreme keel depths from submarine sonar data. *Cold Regions Sci. & Technol***., 6,** 257-266.

Wadhams, P. (1988). The underside of Arctic sea ice imaged by sidescan sonar. *Nature, Lond.,* **333**, 161-164.

Wadhams, P. (2000). *Ice in the Ocean.* Taylor and Francis, 368pp.

Wadhams, P. (2008). Arctic sea ice changes under global warming. Proc. ICETECH 2008, Intl. Conf. on Performance of Ships and Structures in Ice, Banff, July 20-23 2008. Soc. Naval Archit. Marine Engrs, ISBN 978-0-9780896-1-0.

Wadhams, P., J.P. Wilkinson and S.D. McPhail (2006). A new view of the underside ofArctic sea ice. *Geophys. Res. Lett.,* **33**, L04501, doi:10.1029/2005GL025131.

Wadhams, P. and M.J. Doble (2008). Digital terrain mapping of the underside of sea ice from a small AUV. *Geophys. Res. Lett.,* **35**, L01501, doi:10.1029/2007GL031921.

Weeks, W.F., A. Kovacs and W.D. Hibler (1971). Pressure ridge characteristics in the Arctic coastal environment. *POAC 71, Proc. 1st Intl. Conf. Port & Ocean Engng under Arctic Condns. ,* Memorial Univ., St. John's, 152-183.

.

Appendix A: Ridge slopes: Detailed tables

Slope parameters for Ridges 1-9. Note that the maximum draft for each slice (first column) is not necessarily that given as the ridge-crest draft in Appendix A, since that latter figure is constrained to be a linear fit (in plan view) to the dominant crest line. Left-hand (LHS) and right-hand (RHS) parameters are given separately. LID is the Level Ice Draft (if detected). -1 indicates that a minimum value or point of inflection was used to delimit the ridge. '0' indicates that the Rayleigh criterion was used to delimit the ridge. 'Angle' gives the linear regression slope for each side of the ridge (degrees, marked in magenta on the following plots). 'Veq' gives the volume equivalent angle (degrees, marked in red on the following plots). 'sLength' gives the slant length of the ridge slope, in metres, used to weight each slope value to obtain the overall result (weighted mean slopes). Also given are the same parameters for the median ridge envelope, shown in Figure 13.

Ridge 1	**Max Draft,**	**LHS**				**RHS**			
Slice #	**m**	**LID**	**Angle**	**Veq**	**sLength**	**LID**	**Angle**	**Veq**	**sLength**
2	32.7	-1	37	28	18.4	4.3	23	18	70.1
4	31.4	0	14	19	48.3	4.2	20	22	53.9
6	29.7	0	12	18	52.3	4.4	19	19	57.9
8	26.0	3.2	21	28	57.6	4.6	16	17	79.9
10	27.3	3.5	16	24	72.0	4.4	16	20	65.6
12	28.7	4.0	14	28	65.2	4.3	19	24	60.4
14	29.3	3.9	18	28	62.9	4.5	19	20	67.5
16	27.9	3.6	18	24	72.0	0	22	24	32.8
Weighted mean slopes			*17*	*25*			*19*	*20*	
Median ridge envelope			*16*	*28*			*20*	*20*	

Ridge 2	**Max Draft, m**	**LHS**				**RHS**			
Slice #		**LID**	**Angle**	**Veq**	**sLength**	**LID**	**Angle**	**Veq**	**sLength**
2	3.7	-1	2	2	3	1.2	5	5	29.5
4	3.4	-1	3	4	6.0	1.2	3	4	35.9
6	3.4	-1	10	11	6.1	1.2	3	4	42.3
8	4.3	-1	5	4	21.6	1.1	5	5	33.9
10	6.0	0	12	6	15.7	1.2	8	7	31.0
12	4.5	0	7	9	15.5	1.2	8	7	27.9
14	4.3	0	8	8	15.5	1.2	6	6	30.9
16	4.6	0	8	6	15.5	1.2	6	6	34.0
18	4.7	0	9	7	18.7	1.2	7	9	24.8
20	4.6	0	22	26	6.4	1.2	6	6	30.1
22	4.5	0	7	6	21.1	0	24	25	6.6
24	4.1	0	6	4	21.0	0	4	3	30.0
26	4.0	0	6	5	18.1	-1	6	5	18.1
28	3.3	0	3	3	29.6	-1	8	7	11.9
30	3.3	0	4	4	24.2	0	8	6	15.2
32	3.5	0	3	3	32.8	0	12	10	9.1
34	3.6	-1	4	5	26.3	0	18	16	6.1
36	3.8	-1	3	4	27.2	0	17	15	6.3
Weighted mean slopes			***6***	***6***			***6***	***6***	
Median ridge envelope			***6***	***5***			***5***	***4***	

Ridge 3	**Max**	**LHS**				**RHS**			
Slice #	**Draft, m**	**LID**	**Angle**	**Veq**	**sLength**	**LID**	**Angle**	**Veq**	**sLength**
4	3.6	-1	3	3	3.9	1.5	11	12	11.8
6	3.4	-1	6	6	3.8	1.4	10	11	11.6
8	3.4	-1	4	4	3.1	1.5	10	10	11.7
10	3.7	-1	6	5	11.6	1.7	8	6	15.6
12	3.5	0	5	4	19.3	-1	9	9	11.7
14	3.4	0	7	7	15.8	0	1	1	47.2
16	3.0	0	2	2	30.8	0	2	3	30.8
18	3.4	0	3	3	27.0	1.4	3	4	30.8
20	3.4	1.5	3	4	34.7	1.3	11	9	11.7
22	3.4	1.5	4	5	22.8	1.3	6	7	19.1
24	4.0	1.4	4	3	34.8	1.2	13	13	11.8
26	3.2	1.3	2	3	34.6	1.3	4	4	23.1
28	2.9	0	2	1	46.2	1.3	5	5	19.3
30	2.7	0	18	18	4.1	1.0	2	4	27.6
32	3.2	0	1	2	34.6	1.2	2	3	42.3
34	3.4	1.6	7	9	15.5	0	3	3	30.8
36	3.8	1.6	7	6	19.4	0	3	3	30.0
38	3.8	1.4	5	4	27.0	-1	4	4	23.1
40	2.7	0	1	2	46.6	-1	4	4	3.9
42	3.1	1.4	2	2	41.8	NP	NP	NP	NP
44	4.0	1.3	6	6	26.2	NP	NP	NP	NP
46	3.5	-1	4	6	18.8	NP	NP	NP	NP
Weighted mean slopes			***3***	***4***			***4***	***5***	
Median ridge envelope			***3***	***3***			***4***	***3***	

Ridge 4	**Max draft, m**	**LHS**				**RHS**			
Slice #		**LID**	**Angle**	**Veq**	**sLength**	**LID**	**Angle**	**Veq**	**sLength**
2	5.0	-1	12	12	4.0	0	9	11	15.9
4	5.2	0	12	8	12.2	1.9	3	3	57.5
6	5.2	1.8	12	10	16.0	0	5	5	29.6
8	5.2	1.7	12	10	18.1	0	5	5	27.7
10	4.7	1.8	10	7	20.0	0	4	5	27.7
12	5.4	1.9	12	13	17.0	-1	5	6	25.0
14	4.8	1.9	12	9	14.8	1.9	5	7	29.1
16	5.2	1.9	11	9	19.0	1.8	5	5	37.4
18	5.1	1.9	7	6	29.2	1.9	4	5	35.3
20	5.1	1.8	7	8	27.1	1.8	4	6	35.3
22	5.3	1.9	7	8	25.8	1.8	4	5	39.5
24	4.8	-1	17	18	8.3	0	6	8	19.9
26	4.9	0	6	5	21.8	0	8	8	17.9
28	4.2	0	10	13	12.6	-1	6	5	12.5
30	4.8	2.1	2	5	40.0	1.9	2	3	61.9
32	4.7	2.0	2	4	52.4	1.9	2	3	60.8
34	5.0	2.1	7	6	28.4	2.0	2	2	88.9
36	5.7	-1	8	7	26.8	0	2	2	79.7
38	5.9	-1	6	9	38.2	-1	9	14	11.5
40	6.1	-1	9	10	27.1	-1	6	7	25.0
42	6.0	-1	8	10	26.7	-1	6	6	22.7
44	5.9	2.1	8	11	23.0	-1	9	10	13.4
46	5.0	1.9	11	10	17.5	-1	4	6	24.9
Weighted mean slopes			*8*	*8*			*4*	*5*	
Median ridge envelope			*7*	*7*			*4*	*3*	

Ridge 5	**Max draft, m**	**LHS**				**RHS**			
Slice #		**LID**	**Angle**	**Veq**	**sLength**	**LID**	**Angle**	**Veq**	**sLength**
2	2.0	1.4	5	5	9.4	NP	NP	NP	NP
4	2.3	1.4	6	7	9.5	-1	5	5	9.5
6	2.4	1.4	6	7	9.4	-1	5	5	14.1
8	2.8	1.5	5	5	14.2	-1	8	7	14.3
10	2.9	1.5	4	4	16.7	-1	7	6	14.4
12	2.8	1.5	6	8	11.9	1.2	5	6	14.2
14	2.6	1.5	6	7	11.9	-1	5	7	14.2
16	2.6	-1	4	4	24.0	-1	5	4	16.8
18	2.7	-1	5	5	16.8	-1	5	5	21.6
20	2.5	-1	2	2	30.7	-1	5	6	16.6
22	2.8	-1	3	3	23.6	1.3	6	6	11.9
24	2.6	-1	2	2	33.5	1.3	6	6	14.4
26	2.7	0	2	2	33.0	0	3	2	23.6
28	2.6	0	1	1	33.0	0	3	4	18.9
30	2.4	0	2	2	28.7	0	3	4	21.6
32	2.3	0	1	2	35.9	0	4	4	16.8
34	2.6	-1	1	2	37.8	-1	4	4	23.7
36	2.7	-1	2	2	33.0	-1	5	5	21.3
38	2.1	-1	1	2	38.3	-1	5	7	12.0
40	2.1	-1	1	1	28.5	-1	3	2	23.8
42	2.1	-1	2	2	18.9	0	4	3	18.9
44	2.0	-1	2	1	7.1	0	3	2	23.8
46	2.0	NP	NP	NP	NP	0	3	2	18.9
Weighted mean slopes			*2*	*3*			*4*	*4*	
Median ridge envelope			*2*	*1*			*4*	*4*	

Ridge 6	Max draft, m	LHS				RHS			
Slice #		LID	Angle	Veq	sLength	LID	Angle	Veq	sLength
2	5.1	NP	NP	NP	NP	1.4	3	3	80.4
4	5.0	NP	NP	NP	NP	1.3	3	5	43.5
6	5.1	NP	NP	NP	NP	1.3	3	3	90.6
8	5.3	-1	4	6	17.9	1.3	3	3	89.6
10	5.6	-1	4	2	25.6	1.3	3	3	84.5
12	5.7	-1	4	3	30.7	1.2	3	3	81.9
14	5.4	0	4	4	37.8	1.2	3	3	80.5
16	5.4	-1	4	4	40.3	-1	3	3	83.1
18	5.5	-1	4	5	45.3	1.1	4	3	70.5
20	5.4	-1	3	2	75.5	-1	4	3	63.0
22	5.5	-1	3	3	65.4	-1	5	6	45.4
24	6.0	-1	3	3	70.5	-1	6	6	45.4
26	5.7	-1	3	3	78.0	-1	5	6	42.9
28	5.3	0	4	6	42.8	-1	4	4	52.9
30	4.9	1.7	4	4	47.8	-1	3	3	65.4
32	4.4	-1	3	4	48.7	-1	2	2	61.4
34	5.2	-1	2	2	76.8	-1	3	3	53.8
36	4.0	-1	2	2	74.2	-1	2	3	56.3
38	4.2	0	1	2	75.4	-1	3	6	20.1
40	4.9	-1	2	2	113.1	-1	3	4	22.7
42	5.4	-1	2	2	115.7	-1	4	4	17.6
44	5.3	-1	2	2	105.6	-1	4	5	12.6
46	5.2	1.1	2	2	113.2	-1	1	4	15.1
Weighted mean slopes			*3*	*3*			*3*	*3*	
Median ridge envelope			*3*	*3*			*3*	*3*	

Ridge 7	Max draft, m	LHS				RHS			
Slice #		LID	Angle	Veq	sLength	LID	Angle	Veq	sLength
2	1.9	-1	4	2	5.4	0	2	2	24.2
4	2.0	-1	2	2	10.8	1.0	2	2	21.5
6	2.0	-1	2	4	16.1	1.0	4	4	13.5
8	2.0	-1	3	4	16.1	1.0	4	3	16.1
10	1.9	-1	3	3	16.1	1.0	4	5	13.5
12	2.0	1.0	3	3	21.5	0.9	5	5	13.5
14	2.1	-1	3	3	24.2	0.9	7	6	10.8
16	2.1	-1	3	3	24.2	0.9	6	7	10.8
18	2.2	-1	5	5	16.2	0.9	6	5	13.5
20	2.1	-1	7	8	10.8	0.9	5	4	16.2
22	2.2	-1	9	8	10.9	0.9	4	4	16.1
24	2.3	1.1	6	5	13.5	-1	4	4	21.5
26	2.4	0	8	11	8.1	-1	4	5	18.8
28	2.3	0	9	11	8.1	-1	4	5	18.7
30	2.4	1.2	8	10	11.0	-1	6	6	13.7
32	2.3	1.1	11	13	8.2	-1	5	4	16.3
34	2.1	-1	9	9	8.1	-1	5	3	8.0
36	1.9	-1	4	4	13.1	NP	NP	NP	NP
Weighted mean slopes			*5*	*5*			*4*	*4*	
Median ridge envelope			*4*	*3*			*4*	*4*	

Ridge 8	Max draft, m	LHS				RHS			
Slice #		LID	Angle	Veq	sLength	LID	Angle	Veq	sLength
2	4.7	0	19	17	8.8	1.4	15	10	12.9
4	3.9	-1	17	22	9.1	1.4	9	6	15.4
6	3.8	-1	10	7	13.1	1.3	10	8	15.2
8	3.5	-1	7	5	17.0	1.4	11	11	10.8
10	3.5	0	12	9	8.7	0	10	7	10.9
12	3.9	0	13	8	10.9	-1	9	8	15.0
14	3.4	0	6	4	17.5	0	6	4	17.5
16	4.6	-1	9	6	15.5	-1	9	8	17.7
18	3.5	1.7	7	5	15.4	-1	7	5	13.2
20	3.5	1.6	7	6	15.4	-1	9	6	11.1
22	3.1	1.6	6	5	13.2	-1	7	7	13.1
24	3.1	1.7	12	8	6.7	-1	8	9	13.2
26	2.9	1.6	7	6	11.0	-1	6	7	13.2
28	3.0	-1	12	14	6.6	-1	7	13	8.6
30	3.1	-1	9	9	11.1	-1	6	7	15.5
32	3.4	1.5	8	15	15.1	-1	7	7	15.1
34	3.4	-1	5	5	26.1	-1	8	8	13.1
36	3.4	-1	6	6	27.4	-1	13	17	6.5
38	3.6	-1	6	5	19.2	1.6	8	11	15.0
40	3.5	1.6	4	4	25.1	-1	10	16	8.5
42	3.7	1.7	4	4	23.4	1.5	11	11	12.9
44	3.7	1.7	6	5	19.6	0	14	12	8.9
46	3.4	1.7	5	7	18.2	NP	NP	NP	NP
Weighted mean slopes			*7*	*7*			*9*	*8*	
Median ridge envelope			*7*	*6*			*9*	*9*	

Ridge 9	Max draft, m	LHS				RHS			
Slice #		LID	Angle	Veq	sLength	LID	Angle	Veq	sLength
2	2.2	1.5	8	15	3.4	0	11	8	6.8
4	2.2	1.4	9	6	7.2	1.0	14	12	5.5
6	2.4	1.4	7	7	7.4	1.0	9	8	9.3
8	2.3	1.4	7	4	7.5	1.0	6	6	13.1
10	2.8	0	7	4	10.0	1.0	7	7	14.1
12	2.6	-1	2	2	27.9	1.0	9	9	10.1
14	2.8	1.4	8	6	10.1	1.0	9	12	10.1
16	2.6	1.5	8	10	8.1	1.1	9	7	10.1
18	2.7	1.4	5	4	16.0	1.1	7	5	12.1
20	2.2	0	2	2	27.9	1.1	4	4	14.0
22	2.3	0	3	4	18.0	1.1	6	4	14.0
24	2.3	0	5	7	12.0	1.0	3	3	20.0
26	2.5	-1	6	7	14.0	1.0	4	5	20.0
28	3.1	1.3	6	5	16.0	1.0	5	7	20.0
30	3.3	-1	5	5	20.0	1.0	5	5	26.0
32	3.8	1.1	6	5	24.1	1.0	5	4	28.0
34	4.5	1.2	10	7	20.2	1.0	5	4	30.0
36	3.9	1.2	6	5	26.0	1.0	10	11	16.2
38	5.0	-1	15	17	12.4	-1	19	20	12.6
40	5.0	-1	15	18	12.4	1.0	17	18	14.6
42	4.6	-1	12	15	14.3	-1	16	19	12.5
44	3.8	1.1	5	6	28.0	-1	9	7	18.2
46	3.3	-1	6	6	19.1	1.0	5	5	24.8
Weighted mean slopes			*6*	*6*			*7*	*7*	
Median ridge envelope			*6*	*6*			*6*	*7*	